

Supplementary Materials

Charge Tunneling along Short Oligoglycine Chains

Mostafa Baghbanzadeh, Carleen M. Bowers, Dmitrij Rappoport, Tomasz Żaba, Mathieu Gonidec, Mohammad H. Al-Sayah, Piotr Cyganik, Alan Aspuru-Guzik, and George M.

Whitesides

* To whom correspondence may be addressed: gwhitesides@gmwgroup.harvard.edu, and aspuru@chemistry.harvard.edu

This PDF file includes:

Materials and Methods
Supplementary Text
Figs. S1 to S14
Schemes S1 to S3
Tables S1 to S5
References

Materials

All reagents were used as supplied unless otherwise specified. Water was purified using a Millipore Q-POD water purification system. Alkanethiols were purchased from Sigma-Aldrich. For the contact electrode, high purity eutectic gallium-indium (EGaIn) was obtained from Sigma-Aldrich and used as supplied. All peptides were stored at $-20\text{ }^{\circ}\text{C}$. Peptides were purchased from Pepmic (<http://www.pepmic.com/>) with $>95\%$ purity. The purity of compounds was checked using ^1H NMR before using (Fig. S1).

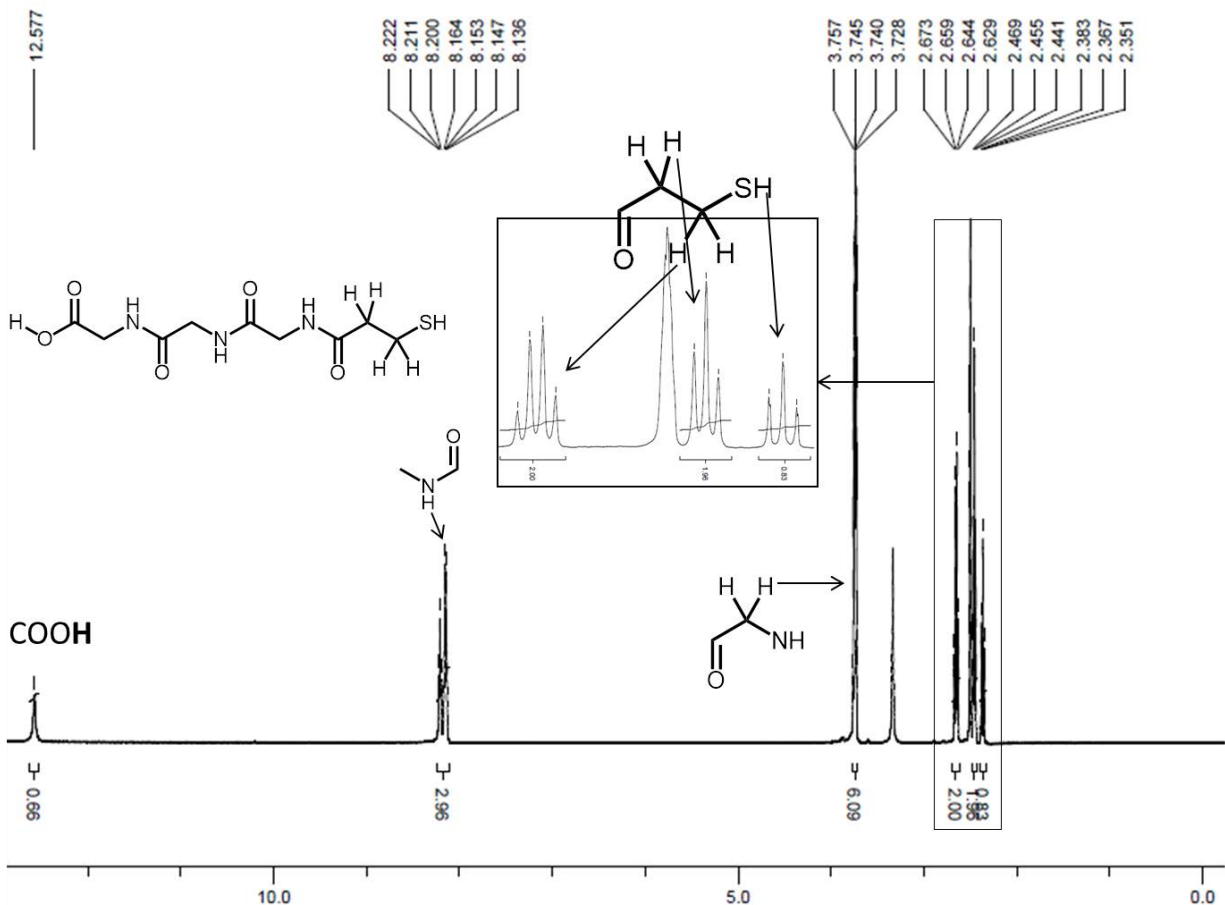
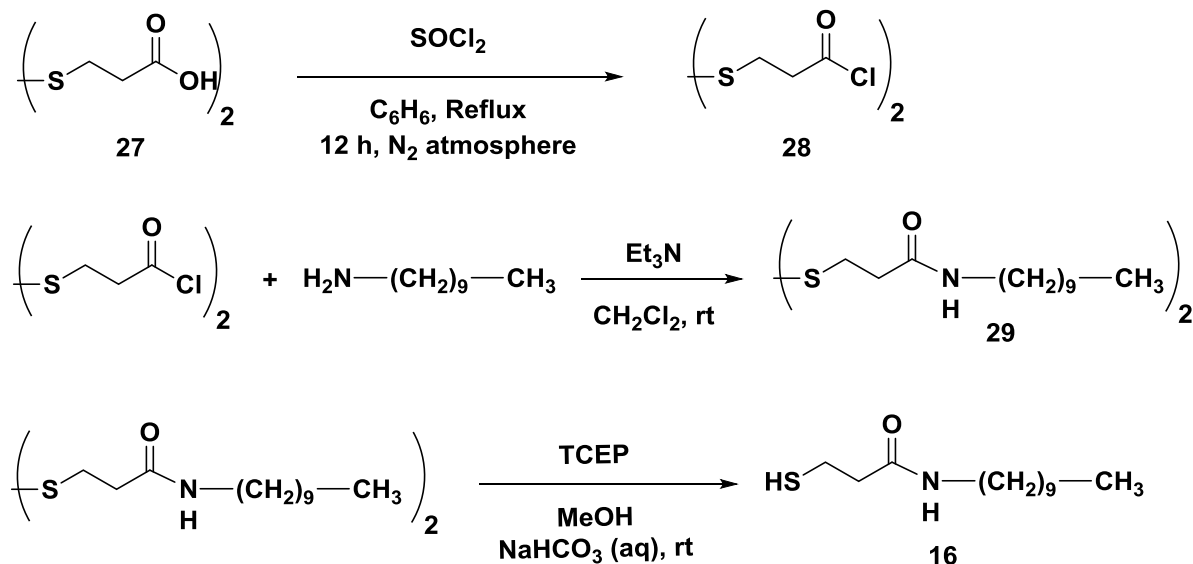


Fig. S1. ^1H NMR spectrum (with peak assignments) of pure compound **20** in $\text{DMSO-}d_6$.

Synthesis of Compound 16

Step 1: Synthesis of Compound 28. (1) 3,3'-Disulfanediyldipropionic acid (**27**) (2 mmol, 420 mg) was added to 20 mL of anhydrous benzene in a round-bottomed flask. Thionyl chloride (40 mmol, 3 mL) was added to the solution. The mixture was stirred for 12 h under reflux condition, and then concentrated by rotary evaporation. The crude residue, containing compound **28**, was used directly in the next step.

Step 2: Synthesis of Compound 16. Decylamine (4 mmol, 0.8 mL) and triethylamine (8 mmol, 1.1 mL) in 20 mL of anhydrous CH₂Cl₂ was added dropwise to a 20-mL CH₂Cl₂ solution of **28** (from step 1) at 0°C. The resulting solution was warmed to room temperature and stirred for 3 h. The reaction solution was filtered, and the solid residue was washed with cold CH₂Cl₂ (3 × 10 mL) and recrystallized from ethanol to give compound **29**. Compound **29** (0.4 mmol, 100 mg) was dissolved in 50 mL of MeOH, followed by addition of a solution of tris(2-carboxyethyl)phosphine (TCEP) (250 mg, 1 mmol) in water (2 mL) and 2 mL of aqueous NaHCO₃ (3M). The mixture was allowed to stir under a nitrogen atmosphere for 5 hours. Water (20 mL) was then added to the mixture and the solution was extracted with CH₂Cl₂ (3 × 30 mL). The combined organic layer was dried (MgSO₄) and evaporated under vacuum to produce the thiol **16** as a white solid in quantitative yield. ¹H NMR (500 MHz, CDCl₃): δ 5.61 (brs, 1H, NH), 3.27 (q, *J*= 6.5 Hz, 2H), 2.82 (q, *J*= 6.5 Hz, 2H), 2.48 (t, *J*= 6.5 Hz, 2H), 1.61 (t, *J*= 6.5 Hz, 1H), 1.50 (m, 2H), 1.38-1.26 (m, 14H), 0.88 (t, *J*= 6.5 Hz, 3H) ppm. ¹³C NMR (125 MHz, DMSO-*d*₆): δ 170.5, 40.5, 39.6, 31.9, 29.6, 29.5, 29.3, 29.2, 26.9, 22.6, 20.5, 14.1. HRMS (ES) calculated for C₁₃H₂₇NOS (MH)⁺: 246.1892; found: 246.1926.



Scheme S1. Synthesis of compound **16**.

Synthesis of Compounds **17** and **18**

Et₃N (8 mmol, 1.1 mL) in 20 mL of CH₂Cl₂ was added dropwise to a mixture of compound **28** (4 mmol) and compound **30** in 20 mL of CH₂Cl₂. After 12 h stirring at room temperature, the mixture was concentrated under vacuum, and the solid residue was recrystallized from CH₂Cl₂ to yield **31** as a white solid powder. Compound **31** was mixed with an excess of amine **32** (4 equiv.) and heated at 60 °C. After 4 h, EtOH (10 mL) was added, the mixture was filtered and the white solid precipitate was washed with EtOH (3 × 10 mL) to give disulfide **33**. Using sonication for 30 min, the disulfide **33** (0.1 mmol) was then dissolved in MeOH (50 mL). A solution of TCEP (120 mg, 0.5 mmol) in water (2 mL) and 2 mL of aqueous NaHCO₃ (3M) were added to the reaction solution, and the mixture was allowed to stir under a nitrogen atmosphere for 5 hours. Water (20 mL) was then added to the mixture, and the solution was extracted with CH₂Cl₂ (3 x 30 mL). The combined organic layer was dried (MgSO₄) and evaporated under vacuum to produce the thiol as a white solid in quantitative yield.

Synthesis of Compound **21**. (Scheme S3)

Synthesis of Compound 34. In a round-bottomed flask, glycylglycylglycine (10 mmol, 1.86 g) was dissolved in 30 mL of methanol (MeOH) and cooled to 0 °C. SOCl₂ (1.1 mL, 15 mmol) was added drop-wise and the reaction mixture was warmed to rt and stirred for 3 h, then concentrated by rotary evaporation. The crude residue was rinsed with diethyl ether (Et₂O) (3×30 mL) to yield compound **34** as a white solid.(2)

Synthesis of Compound 21. In a round-bottomed flask, compound **28** (2 mmol) and compound **34** (4 mmol, 800 mg) were added to 20 mL of CH₂Cl₂ and stirred vigorously (1000 rpm). Triethylamine (8 mmol, 1.1 mL) was dissolved in 20 mL of CH₂Cl₂, and added to the mixture drop-wise. After stirring for 24 h at room temperature, the mixture was filtered and the white solid residue was washed with ethanol (EtOH) (3×20 mL) to yield compound **35** as a white solid powder. Using a sonicator for 30 min, the disulfide **35** (60 mg, 0.11 mmol) was then dispersed in methanol (50 mL) (Note: the solubility of compound **35** in methanol is low, and even after sonication the solution does not become clear). Solution of TCEP (125 mg, 0.5 mmol) in water (2 mL), and 2 mL of aqueous NaHCO₃ (3M), were added to the reaction solution and the mixture was allowed to stir under nitrogen atmosphere for 5 hours. Water (20 mL) was then added to the mixture and the solution was extracted with CH₂Cl₂ (3 × 30 mL). The combined organic layer was dried (MgSO₄) and evaporated under vacuum to produce the thiol **21** as a white solid in quantitative yield. ¹H NMR (500 MHz, DMSO-*d*₆): δ 8.27 (t, *J* = 6 Hz, 1H, NH), 8.17-8.12 (m, 2H, 2 NH), 3.84 (d, *J* = 6 Hz, 2H), 3.73 (d, *J* = 6 Hz, 2H), 3.70 (d, *J* = 6 Hz, 2H), 3.62 (s, 3H, OCH₃), 2.65 (q, *J* = 6 Hz, 2H), 2.65 (t, *J* = 6 Hz, 2H), 2.35 (t, *J* = 6 Hz, 1H) ppm. HRMS (ES) calculated for C₁₀H₁₈N₃O₅S (MH)⁺: 292.0967; found: 292.1025.

Methods

Forming SAMs of Polypeptides on Au.^{TS} Cysteine is commonly used to immobilize peptides on gold surfaces. We selected glycine (Gly) as the repeating peptide residue, because it is structurally the simplest amino acid. Oligoglycines (Cys(Gly)_n)—having a terminal cysteine residue and glycine units (n) ranging from n = 1 to n = 5—are all commercially available (Pepmic (<http://www.pepmic.com/>), >95% purity). SAMs on template-stripped gold (Au^{TS}) were prepared according to protocols previously reported by us and others.⁽³⁾ In brief, the SAMs were formed by submerging the Au surface in a 1mM solution of peptide in degassed water for 12-18 hours at room temperature under a nitrogen atmosphere. After incubation, the Au^{TS}-SAM samples were rinsed through immersion, for three minutes each, in three separate vials containing filtered, deionized water (H₂O). The SAM-bound surface was then rinsed with a stream of ethanol and allowed to dry in air. To determine the sensitivity of the measured current density to the rinsing protocol, we also measured charge transport across SAMs that were rinsed using streams of water and ethanol, and dried under nitrogen. We observed no difference in current density between the two protocols.

Characterization of the Structure of SAMs using XPS. X-ray photoelectron spectroscopy (XPS) was performed with a photoelectron spectrometer (K-Alpha XPS System, Thermo Scientific) equipped with a hemispherical analyzer. The spectra were acquired using a monochromatized aluminum source Al K_a (E= 1486.6 eV); the base pressure in the analytical chamber was ~10⁻⁹ mbar. The spectra were acquired using a standard emission geometry with an analyzer energy resolution of 0.1 eV. The inelastic background was subtracted using the Shirley method and the photoemission peaks were fit using Gaussian and Lorentzian functions

with adjustable weights. The identification of the XPS peaks was based on recent XPS(4) and HRXPS(5, 6) data obtained for oligopeptides and cysteine.

Fig. S2 shows XPS spectra (regions of C1s, O1s, N1s and S2p) acquired for SAMs of Cys(Gly)₅ on Au(111). The S2p region was fitted with a set of two doublets centered at 162 eV and 161.3 eV; both doublets confirm the formation of a Au-S bond. (A S2p signal at 164 eV would be indicative of physisorbed Cys(Gly)₅ molecules, which has been documented previously using HRXPS studies of cysteine on Au(111) and Ag(111)(5, 6)). The doublet centered at 162 eV is associated with the formation of a thiolate bond with gold (5, 7). The signal centered at 161 eV has been observed previously for thiol-based SAMs, (7, 8) including those based on cysteine, (5) and has been ascribed to three possible scenarios: the presence of atomic sulfur, the adsorption of thiolate species that are different from the main component of the SAM, and thiolates that are bound in a different S-Au(111) configuration. (5, 8)

For SAMs of Cys(Gly)_n, the intensity of this additional component at 161 eV is high and contributes to ca. 30-40% of the total S2p signal. Attributing this signal to atomic sulfur or thiolate species, which are different from the target molecules, would imply a disordered structure of the SAM. This assumption is in contrast to our analysis of film thickness by XPS and Ellipsometry, which confirm the formation of well-defined SAMs of Cys(Gly)_n, and the IRRAS data, which confirms the formation of secondary structure characteristic of peptides. Therefore, we attribute, as we have in previous work,(7, 8) that this additional S2p component at 161.3 eV is due to a different S-Au(111) binding configuration. This conclusion is supported by a combination of HRXPS and STM data obtained for Cys/Ag(111),(6) where the formation of two different surface structures is associated with a shift in the S2p doublet.

The C1s region can be fitted with three peaks: 288.2 eV, COOH/C=O; 286.3 eV, C-N; 284.6 eV, C-C. A component of the C1s signal at 284.6 eV could be attributed to adventitious carbon and oxygen (9), to which type of contamination hydrophilic monolayers of peptides are particularly prone (9). Atmospheric contamination could also contribute to the C1s signal at 288.2 eV (corresponding to the COOH/C=O binding) and to the O1s region, which has two peaks centered at 533.5 eV (COOH) and 531.7 eV (C=O). The C1s and O1s signals that arise from contamination on the surface give strong XPS signals due to the lack of attenuation in these signals by molecular material on top of them. In contrast to superficial contamination, signals originally in SAMs that are adsorbed as ordered structures on a surface result in signals from atoms deeper in the monolayer that attenuate with thickness. The N1s region shows two peaks at 401.9 eV and 400.1 eV; previous HRXPS analysis of Cys adsorption on Au(111) (5) and Ag(111) (6) attributed these signals to NH_3^+ and NH_2 . The presence of NH_3^+ is due to the formation of a zwitterion within the peptide structure. The ultra-high vacuum environment excludes the possibility for a reaction between the amine and atmospheric CO_2 , which otherwise might lead to the detection of NH_3^+ . In contrast to the C1s and O1s signal, the N1s signal can be attributed exclusively to the peptide layer since the amide group is not a common atmospheric contaminant. Fig. S3 shows the evolution of N1s signal along the series of SAMs of $\text{Cys}(\text{Gly})_n$ ($n = 0-5$) molecules. The total area of the N1s peaks increases monotonically with the length of $\text{Cys}(\text{Gly})_n$, indicating an increase in the effective thickness of SAMs (from $n = 0$ to $n = 5$). The change in the relative intensity of the 401.9 eV and 400.1 eV peaks for a SAM of Cys is due (possibly) to a change in the protonation state of the amide group from NH_2 to NH_3^+ . (5, 6) Since the N1s signal is characteristic of the $\text{Cys}(\text{Gly})_n$ series, and remains unaffected by adventitious contamination, we used N1s to estimate the effective thickness by comparing the intensity of the

N1s and Au4f signal (this method was used in previous work(10) for SAMs of alkanethiols on surfaces of gold). We used this approximation to analyze the relationship between the effective film thickness and the parameter “n” in Cys(Gly)_n (n = 0-5), rather than determine directly the thickness of the SAMs. As shown in Fig. S4A, there is a linear relationship between the effective film thickness and the parameter “n”. The effective film thickness is 30% smaller for the longest compounds (although the values for XPS and ellipsometry are similar for shorter compounds) than that expected from a calculated thickness, and that estimated by ellipsometry. This difference in effective film thickness (estimated by XPS) and calculated molecular length (estimated using an all *trans*-extended conformation) could be attributed to the presence of intermolecular hydrogen bonds and the formation of secondary structure (perhaps in the form of beta-sheets).

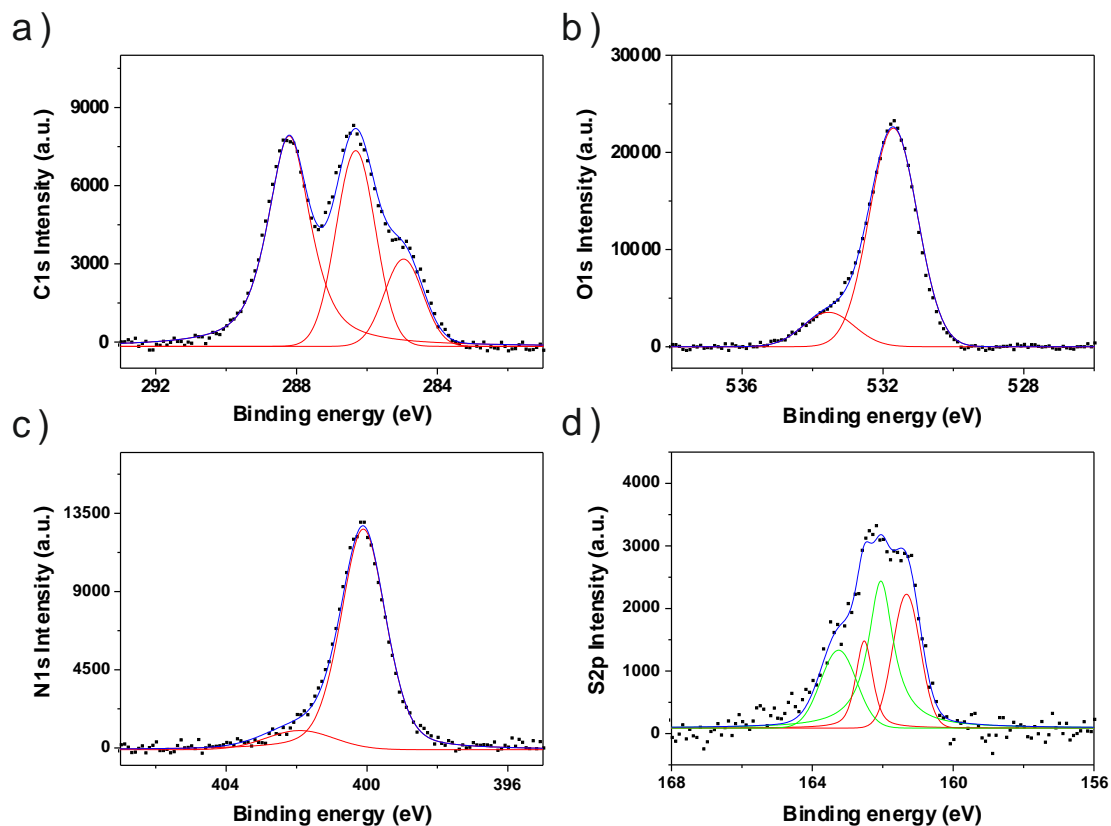


Fig. S2. XPS spectra of Cys(Gly)₅ sample. a) C1s region with peaks at 288.2 eV, 286.3 eV and 284.6 eV representing carbon atoms in COOH/C=O, C-N, and C-C. b) O1s region with two peaks at 533.5 eV and 531.7 eV representing oxygen atoms in COOH and C=O. c) N1s region with peaks at 401.9 eV and 400.1 eV representing nitrogen atoms in NH₃⁺ and NH₂ configuration. d) S2p region with two doublets at 162 eV and 161.3 eV.

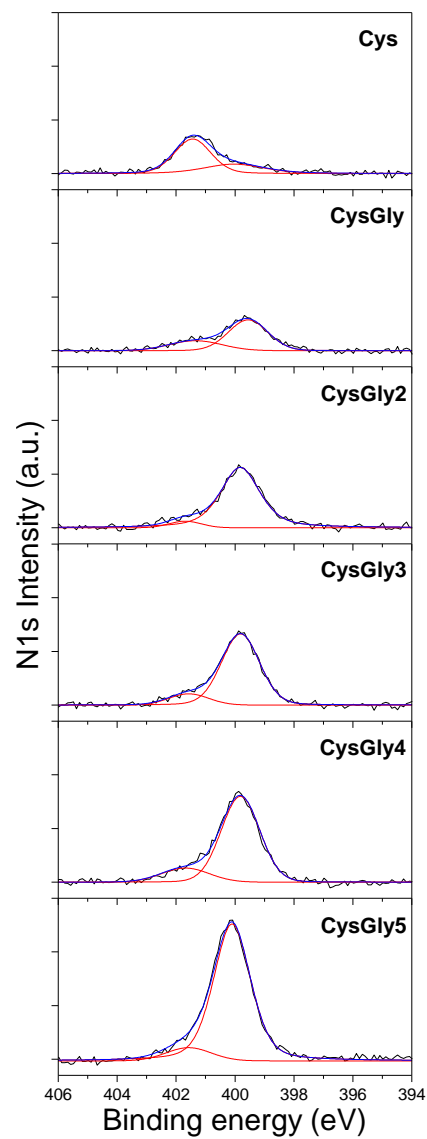


Fig. S3. XPS spectra in the N1s region for Cys(Gly)_n ($n = 0-5$). Peaks at 401.9 eV and 400.1 eV correspond to NH_3^+ and NH_2 .

Measurements of the Thickness of SAMs using Ellipsometry. Thicknesses of SAMs of oligoglycines were measured at a constant angle of incidence of 70° using a single-wavelength scanning ellipsometer (LSE-W model, Gaertner Scientific); the spectroscopic results were simulated using the LGEMP software provided by the manufacturer (index of refraction between 1.46 and 1.48). To compensate for the possibility in heterogeneity in thickness and composition across the surface, measurements were taken at ten different positions across two different substrates. The results, summarized in Fig. S4B, indicate that the thicknesses of SAMs of oligoglycines are comparable with those calculated for SAMs of oligoglycines on gold with a tilt angle of 30° . Measurements on SAMs of alkanethiolates on surfaces of gold serve as a standard, and are comparable with previous reports on thickness obtained using ellipsometry.⁽¹¹⁾ These measurements do not define the detail of the structure of these SAMs, but are compatible with a trans-extended conformation for the derivatives of oligo(gly)_n with an $\sim 30^\circ$ tilt.

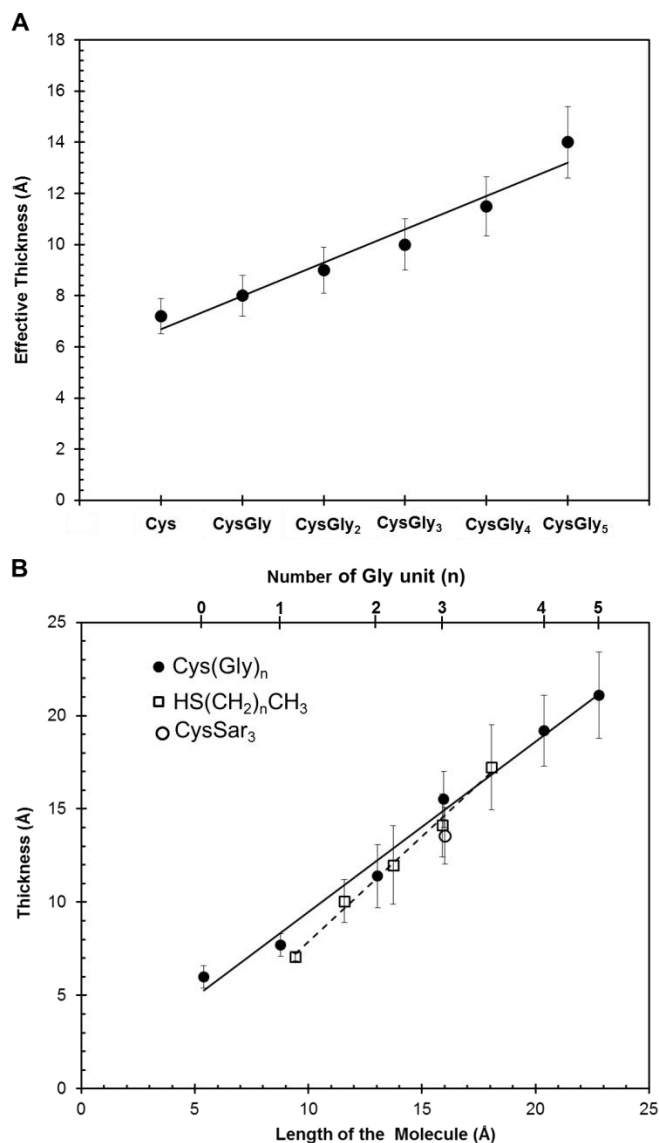


Fig. S4. A) Plot of effective film thickness (based on the N1s signal from XPS) as a function of “n” from the Cys(Gly)_n ($n = 0-5$) series. The solid line is a linear fit to these data. B) Plot of thickness for SAMs (measured using ellipsometry) of Cys(Gly)_n ($n = 0-5$) as a function of length of the molecule (solid line). The dashed line shows the thickness of SAMs of standard alkanethiolates on gold. These values are in agreement with previously reported values for alkanethiolates on gold.

Characterization of the Structure of SAMs using IRRAS. IR reflection absorption spectroscopy measurements were performed with a dry-air-purged Thermo Scientific FTIR spectrometer (Nicolet 6700), which is equipped with a liquid nitrogen-cooled MCT detector. All spectra were taken using p-polarized light incident at a fixed angle of 80° with respect to the surface normal. Spectra were measured at a resolution of 2 cm^{-1} and are reported in absorbance units $A = -\log R/R_0$, where R is the reflectivity of the substrate with the monolayer and R_0 is the reflectivity of the reference. Substrates covered with a SAM of perdeuterated hexadecanethiolate were used as a reference.

Fig. S5 shows the evolution of the IRRAS spectra in the Amide I ($1600 - 1700\text{ cm}^{-1}$; C=O stretching) and Amide II ($1480 - 1600\text{ cm}^{-1}$; CN stretching, NH bending) region along the series of SAMs of Cys(Gly)_n (n = 1-5).⁽¹²⁾ Broadening of peaks in the Amide I and Amide II region is caused by the multicomponent structure of the peaks. Each of the components can be attributed to the secondary structure of the peptides, and is well known for IR studies in the solid phase. Due to surface selection rules, the intensity proportionality between components is strongly modified in the analysis of infrared reflection absorption, which is in contrast to transmission IR spectra. Hence, we used a simple method for data analysis by integrating the signal over the extended Amide I and Amide II range (from 1800cm^{-1} to 1480cm^{-1}) (Fig. S6). An odd-even oscillation in the integrated IRRAS signal is evident. This odd-even effect is a consequence of alternating the orientation of the consecutive Gly units with respect to the metal substrate, and indicates that short sequences of oligoglycines adopt a polyglycine I structure. This structure has been identified for Gly_n (n=1-5) in the solid state, but has not previously been identified experimentally in a SAM.

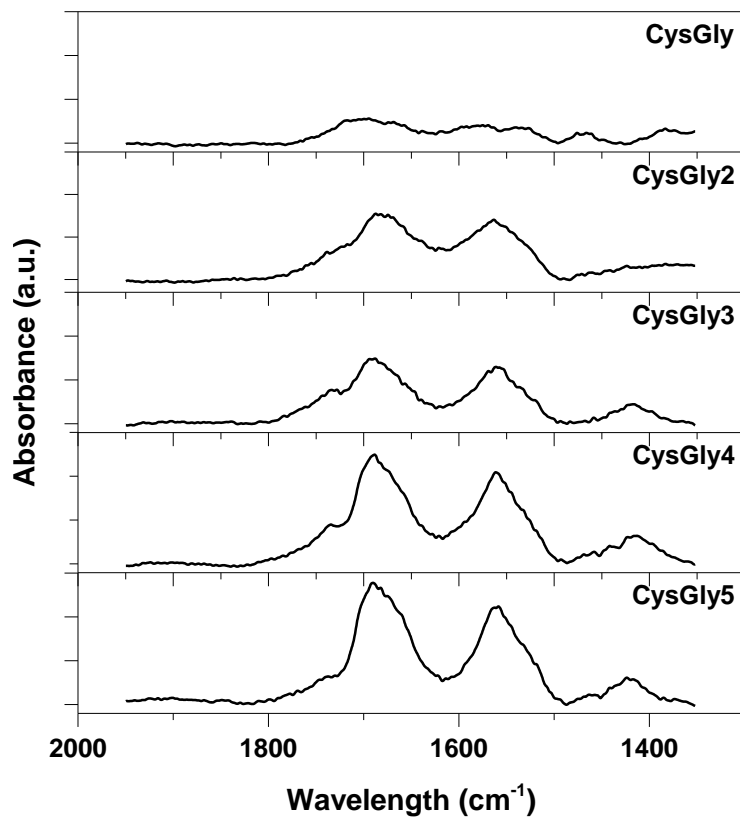


Fig. S5. IRRAS spectra of amide I region of peptide samples with different Gly units number (1-5). Bands inside of the region ranging from 1700 to 1480 cm⁻¹ are associated with vibrations of C=O, C-N and N-H bonds.

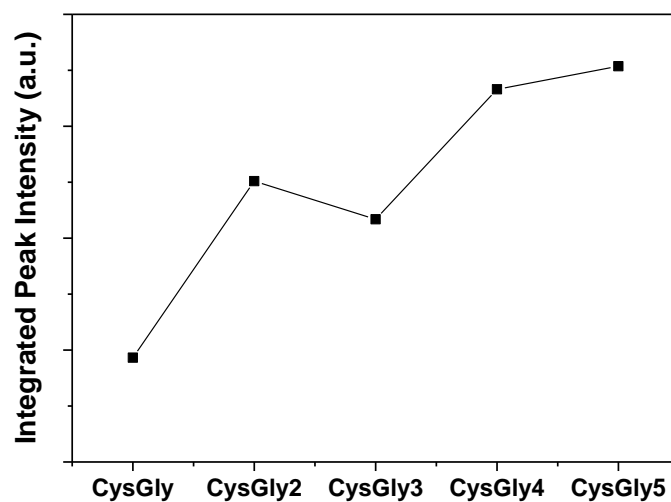


Fig. S6. Plot of integrated IRRAS signal over the range of 1800cm^{-1} to 1480cm^{-1} for SAM samples of molecules with different Gly units number (1-5). Solid line is a connection between data points and it was used to emphasize odd-even oscillations of the IRRAS data.

Presence of Secondary Structure in SAMs of Cys(Gly)_n. The secondary structure of polyglycine (PG), which forms due to the formation of intra- and intermolecular networks of hydrogen bonds between CO and NH groups, are known as PGI and PGII, and have been identified in both the crystalline (13-15) and liquid phase of PG.(16-18) Short oligoglycines (Gly)_n (n ≤ 5) in the solid phase adopt the PGI structure. It was assumed, with no experimental evidence, that SAMs of (Gly)_n (n ≤ 5) on Au(111) also exhibit PGI structure.(19) Here we observe an odd-even effect in the IRRAS data, which results from odd-even changes in the conformation of consecutive Gly units within the SAMs of Cys(Gly)_n, and is indicative of the formation of β-sheets in the PGI structure. Similarities in the structure of molecules present in a SAM, and in the solid state, have been reported previously for systems with strong intermolecular interactions (i.e., aromatic molecules). Therefore, the observation made here for SAMs of oligoglycine, where strong intermolecular interactions via hydrogen bonding lead to the formation of secondary structure, is not surprising. We conclude from the experimental data that SAMs of Cys(Gly)_n (n = 0-5) exhibit beta-sheet structures and analysis by XPS and ellipsometry confirms that these structures grow linearly with an increase in the number of glycine residues.

In summary, our analysis of film thickness (using both XPS and Ellipsometry) and secondary structure (using IRRAS) is compatible with the formation of well-ordered SAMs of Cys(Gly)_n on gold.

Table S1. Summary of static water-wetting contact angles (θ_s) on Au^{TS}.

SAM ^a on Au ^{TS}	mean static contact angle (θ_s) and standard deviation
2	wetted
6	wetted
14	57 ± 2
16	98 ± 2
17	74 ± 1
18	80 ± 2
19	44 ± 2
21	65 ± 1

^aThe numbers correspond to compounds in Fig. 1 and 3A.

Data Collection. We formed SAMs on template-stripped Au^{TS} substrates.⁽³⁾ We used “selected conical tips” as top-electrodes on Au^{TS}-SAM substrates.⁽²⁰⁾ To form stable contacts, we brought the tips closer to the substrates until we could clearly observe (by optical microscopy) the tip apex wrinkling or deforming (for detailed information on the formation and use of conical tips, see the video in the supporting information of ref. 3).⁽³⁾ We have followed a standard procedure for data acquisition, which we call the “1/1/20” protocol. For each individual tip, we formed one junctions (i.e., contacts), and we recorded 20 $J-V$ traces for forward bias ($V = -0.5 \text{ V} \rightarrow V = +0.5 \text{ V}$) and 20 $J-V$ traces for reverse bias ($V = +0.5 \text{ V} \rightarrow V = -0.5 \text{ V}$). We use this procedure to avoid using a tip contaminated with absorbed impurities.

n-Alkanethiolates as Standards. Simple *n*-alkanethiolates on Au^{TS} serve as internal standards for comparison. Junctions of the structure Au^{TS}/S(CH₂)_nH//Ga₂O₃/EGaIn ($n = 5-18$) are, by now, well-characterized and increasingly well-understood.⁽³⁾ The charge tunneling across SAMs is typically modeled by a simple form of the Simmons equation (eq. 1) and the values of both J_0 and β for *n*-alkanethiolates are available for a variety of large-area and single-molecule junctions.⁽²¹⁾

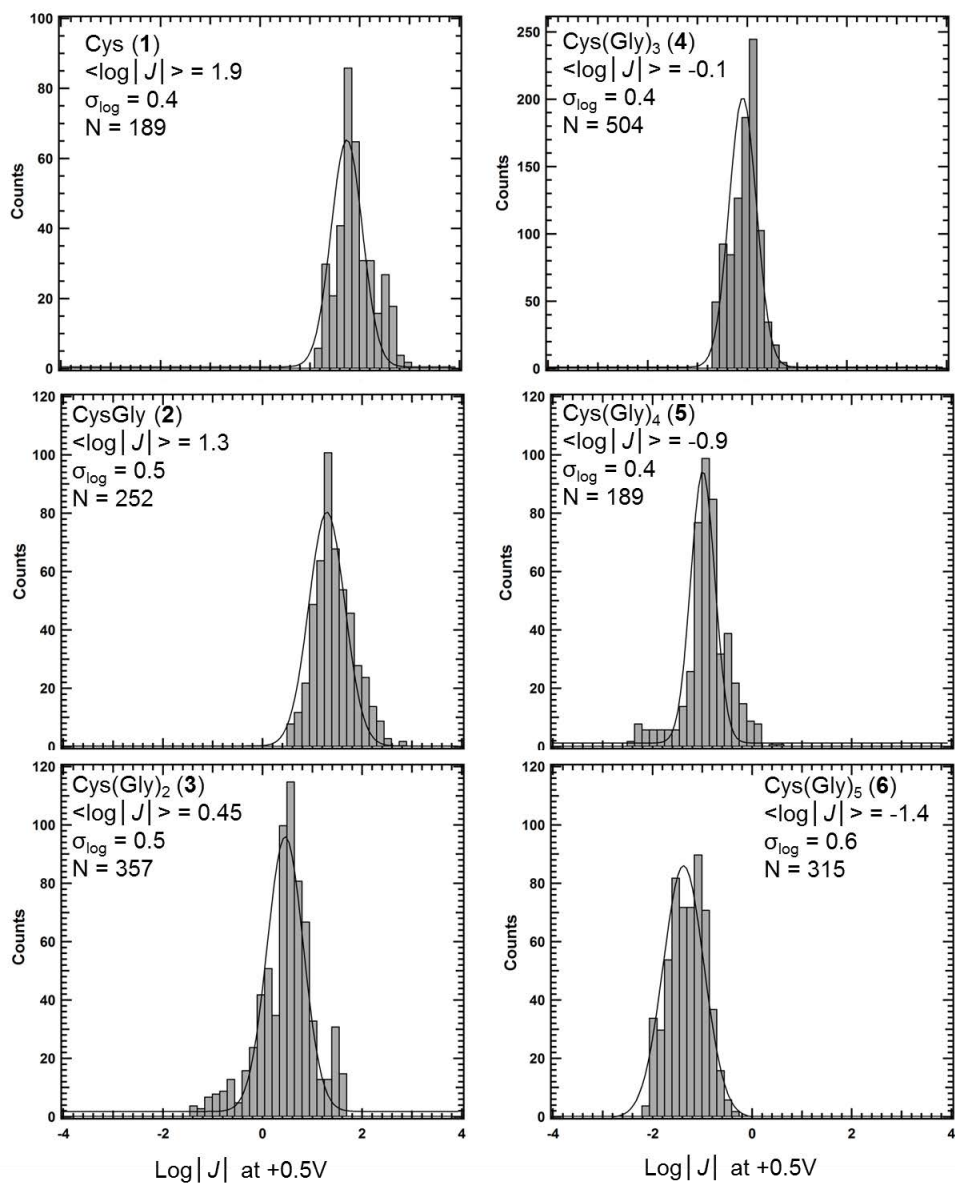


Fig. S7. Histograms of current densities (at +0.5V) of the peptides from Fig. 1 ($\log|J|$: log scale of current density; σ_{\log} : log scale of standard deviation of J).

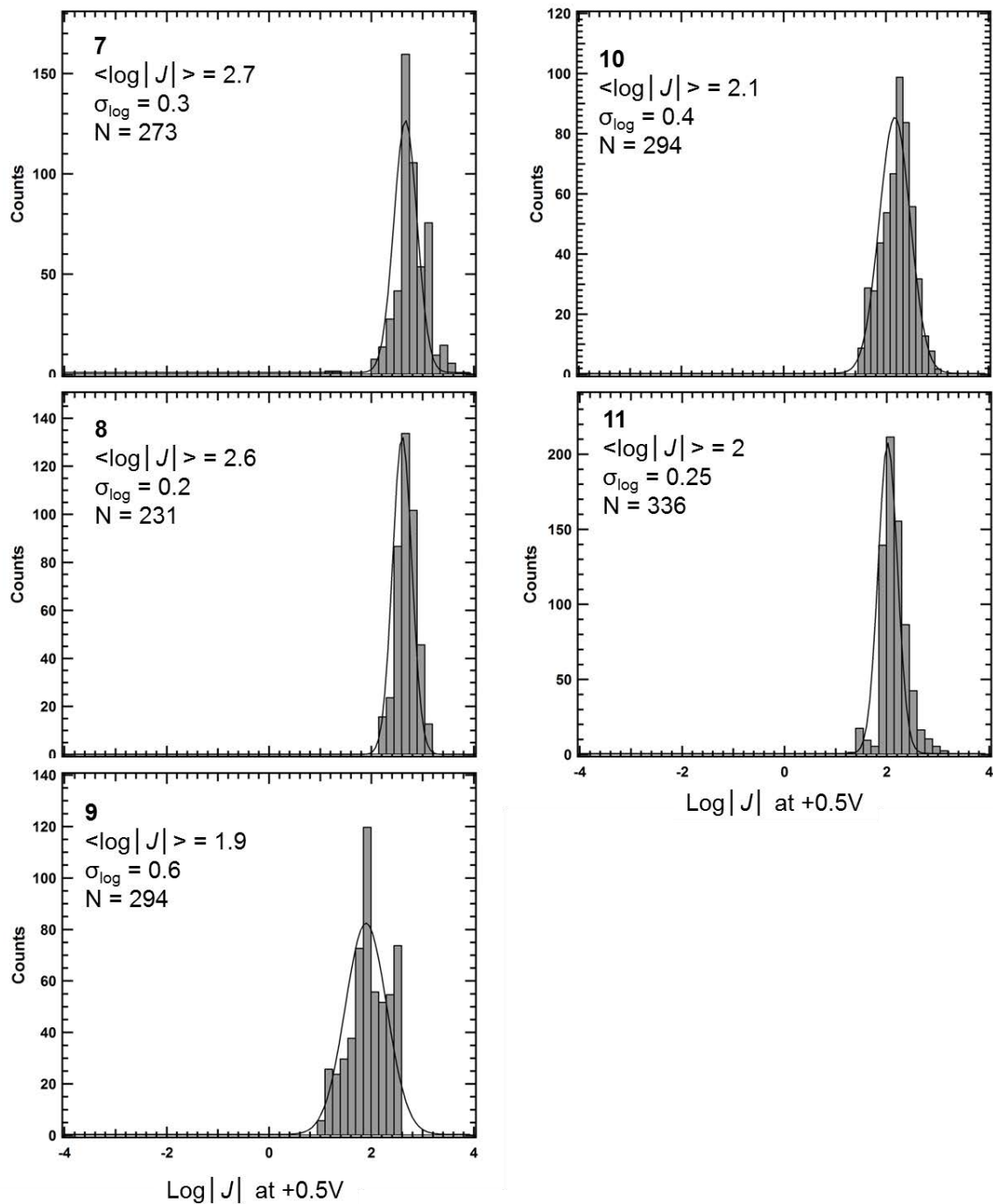


Fig. S8. Histograms of current densities (at +0.5V) of compounds **7-11** from Fig. 2. ($\log |J|$: log scale of current density; σ_{\log} : log scale of standard deviation of J). The presence of a free amine group does not influence the current density.

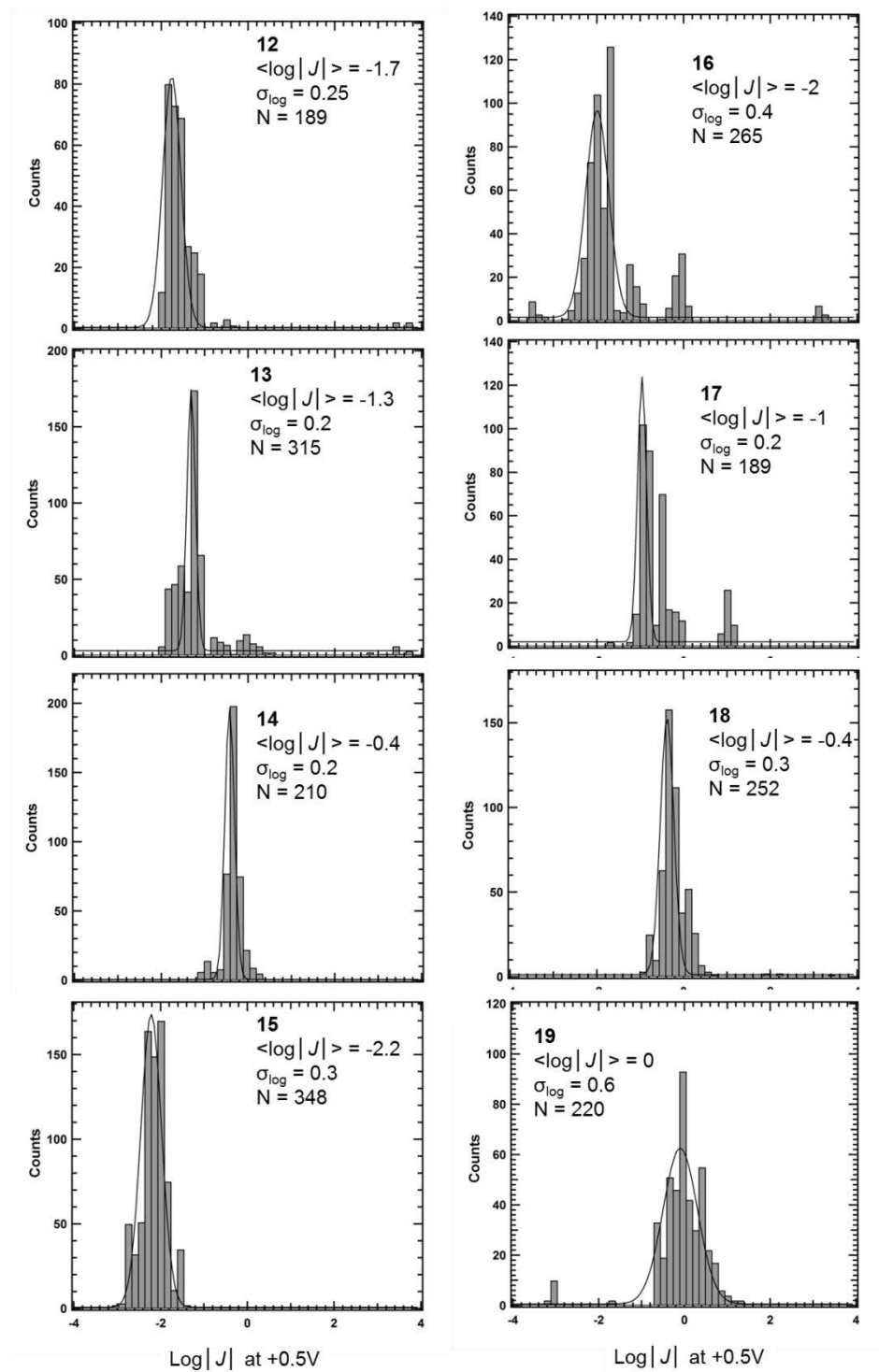


Fig. S9. Histograms of current densities (at +0.5V) of compounds **12-19** from Fig. 3. ($\log |J|$: log scale of current density; σ_{\log} : log scale of standard deviation of J).

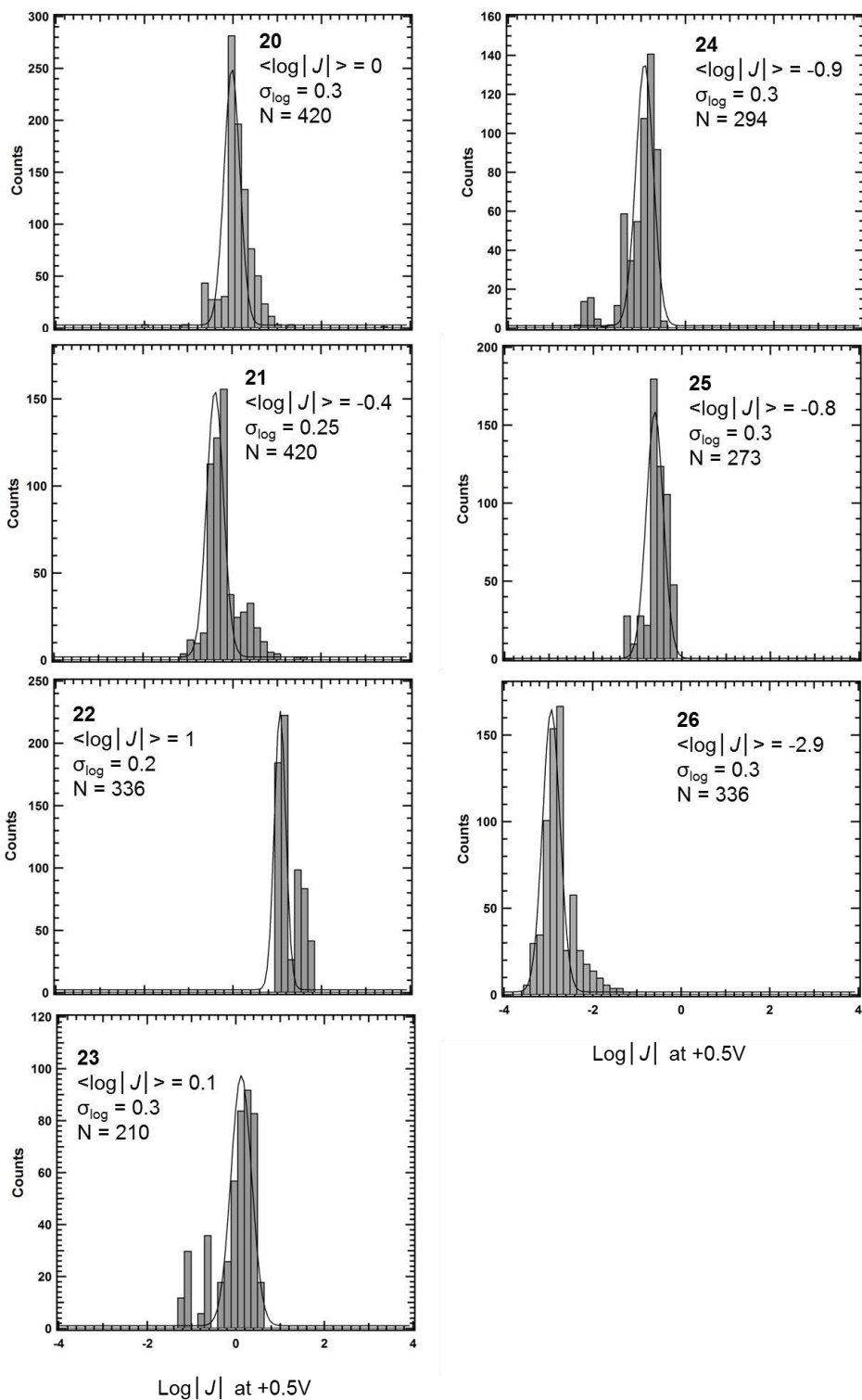


Fig. S10. Histograms of current densities (at +0.5V) of compounds **20-26** from Fig. 3. ($\log|J|$: log scale of current density; σ_{\log} : log scale of standard deviation of J).

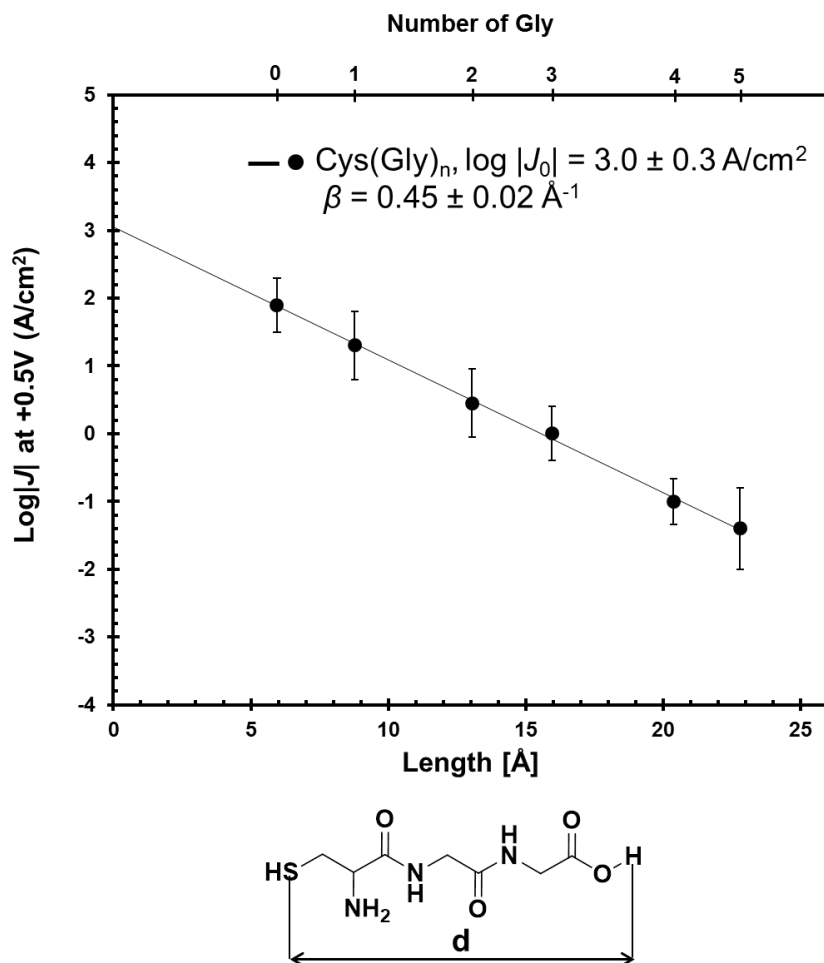


Fig. S11. Plot of the Gaussian mean values of $\log|J|$ at +0.5 V *versus* molecular length for oligoglycines using a junction with the structure Au^{TS}/SAM//Ga₂O₃/EGaIn. Length represents the distance between sulfur and most distal hydrogen assuming all-trans conformation, and were obtained from DFT structure optimizations (see text). Error bars represent the standard deviation of Gaussian mean values.

Computational Details. We performed density functional calculations on cluster models of gold-bound oligoglycines and their structural analogs using the B3LYP hybrid exchange-correlation functional⁽²²⁾ and the resolution-of-the-identity approximation for the Coulomb interaction.⁽²³⁾ We employed split-valence plus polarization basis sets,⁽²⁴⁾ along with the corresponding auxiliary basis sets,⁽²⁵⁾ and small-core relativistic effective core potentials for Au throughout.⁽²⁶⁾ We carried out unrestricted structure optimizations on oligoglycines and their structural analogs attached to the Au₁₀ metal clusters. Subsequently, we analyzed the orbital energies and orbital shapes of the molecular orbitals (MOs) of the metal–molecule complexes at their respective optimized structures. Due to the presence of an unpaired electron on the Au₁₀ cluster, the spin-up (alpha) and spin-down (beta) orbitals of the gold-bound oligoglycines, there are subtle differences in the orbital energies (Tables S2–S4 shows the spin-up and spin-down orbitals separately). The orbital energies in Fig. S12–S14 are an average of the corresponding spin-up and spin-down orbital energies. All computations were performed using TURBOMOLE quantum chemical program suite.⁽²⁷⁾

Table S2. Sulfur lone pair orbitals in neutral Au₁₀Cys(Gly)_n (n = 0-5) clusters. Spin-up (alpha) and spin-down (beta) MOs are shown separately.

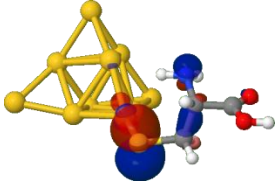
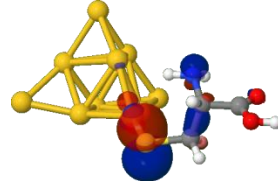
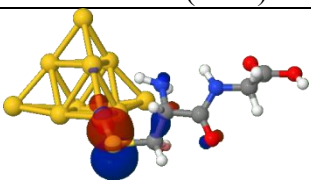
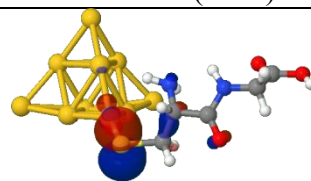
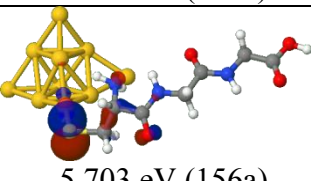
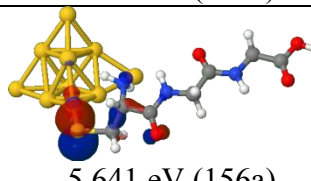
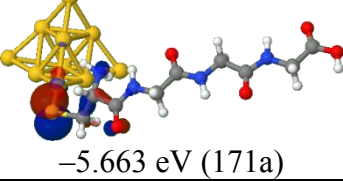
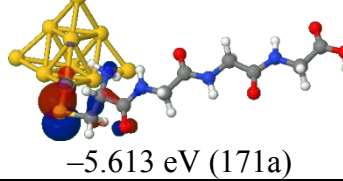
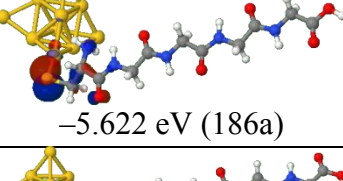
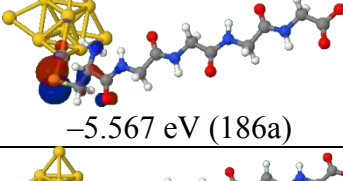
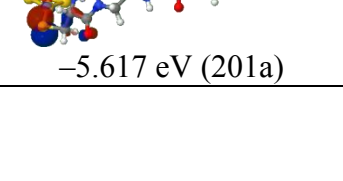
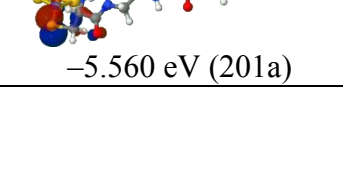
Compound	MO, S alpha	MO, S beta
Au ₁₀ Cys	 -5.789 eV (126a)	 -5.751 eV (126a)
Au ₁₀ CysGly	 -5.785 eV (141a)	 -5.736 eV (141a)
Au ₁₀ Cys(Gly) ₂	 -5.703 eV (156a)	 -5.641 eV (156a)
Au ₁₀ Cys(Gly) ₃	 -5.663 eV (171a)	 -5.613 eV (171a)
Au ₁₀ Cys(Gly) ₄	 -5.622 eV (186a)	 -5.567 eV (186a)
Au ₁₀ Cys(Gly) ₅	 -5.617 eV (201a)	 -5.560 eV (201a)

Table S3. In-plane occupied orbitals of the amide groups in neutral Au₁₀Cys(Gly)_n (n = 1-5) clusters. Spin-up (alpha) and spin-down (beta) MOs are shown separately.

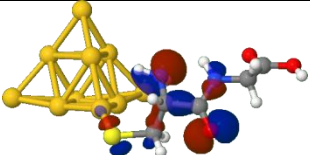
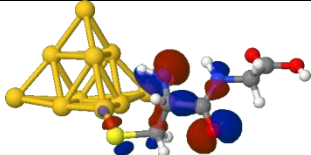
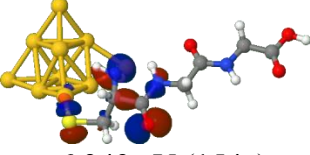
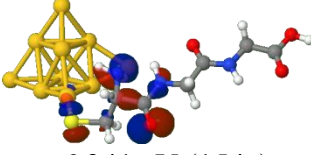
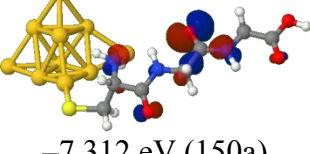
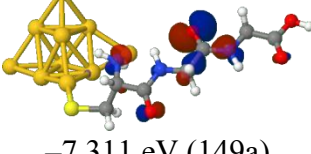
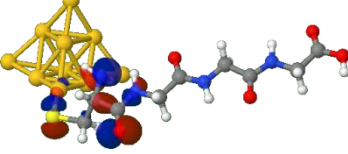
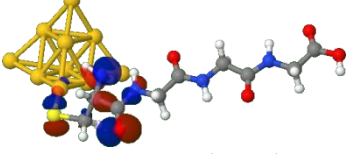
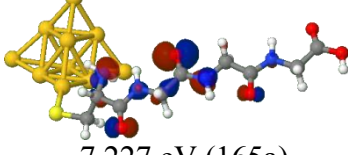
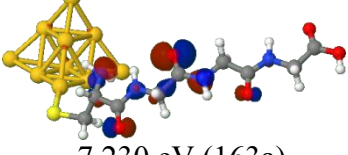
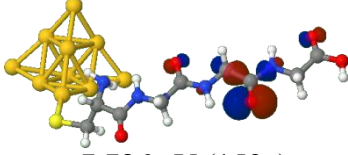
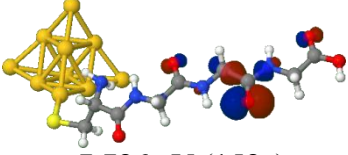
Compound	MO, O alpha	MO, O beta
Au ₁₀ CysGly	 -6.642 eV(139a)	 -6.638 eV (139a)
Au ₁₀ Cys(Gly) ₂	 -6.349 eV (154a)	 -6.341 eV (154a)
	 -7.312 eV (150a)	 -7.311 eV (149a)
Au ₁₀ Cys(Gly) ₃	 -6.300 eV (169a)	 -6.292 eV (169a)
	 -7.227 eV (165a)	 -7.230 eV (163a)
	 -7.786 eV (159a)	 -7.786 eV (158a)

Table S3 (continued).

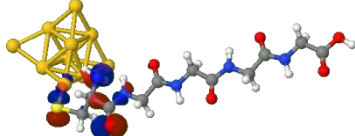
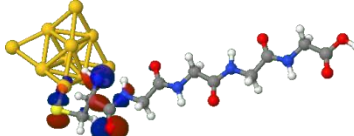
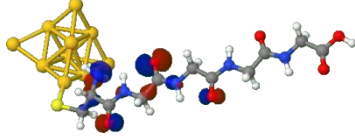
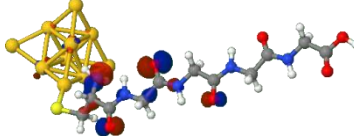
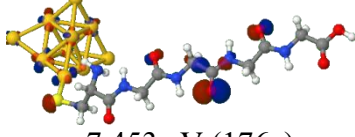
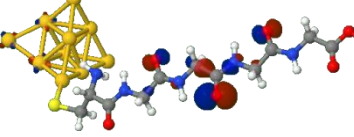
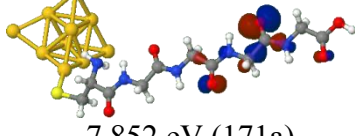
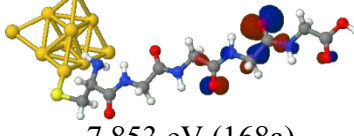
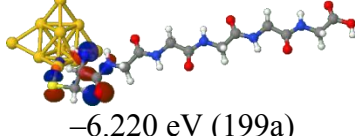
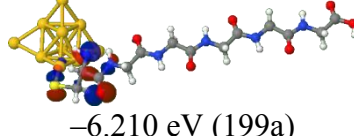
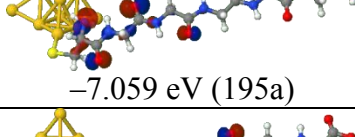
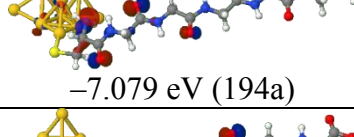
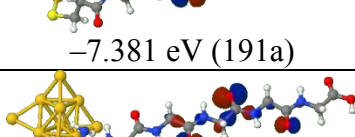
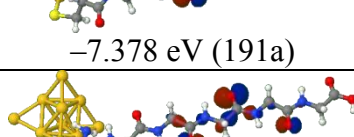
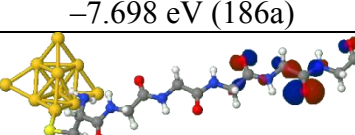
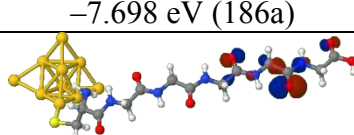
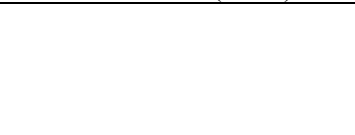
Compound	MO, O alpha	MO, O beta
Au ₁₀ Cys(Gly) ₄	 -6.223 eV (184a)	 -6.213 eV (184a)
	 -7.084 eV (180a)	 -7.098 eV (179a)
	 -7.453 eV (176a)	 -7.468 eV (175a)
	 -7.852 eV (171a)	 -7.853 eV (168a)
Au ₁₀ Cys(Gly) ₅	 -6.220 eV (199a)	 -6.210 eV (199a)
	 -7.059 eV (195a)	 -7.079 eV (194a)
	 -7.381 eV (191a)	 -7.378 eV (191a)
	 -7.698 eV (186a)	 -7.698 eV (186a)
	 -8.052 eV (179a)	 -8.052 eV (179a)

Table S4. Out-of-plane occupied orbitals of the amide groups in neutral Au₁₀Cys(Gly)_n (n = 1-5) clusters. Spin-up (alpha) and spin-down (beta) MOs are shown separately.

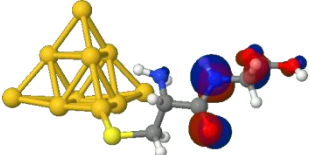
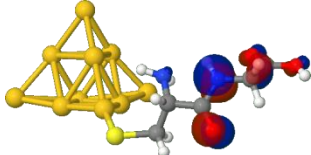
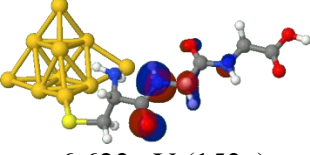
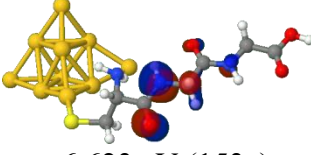
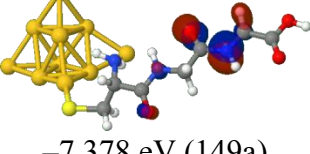
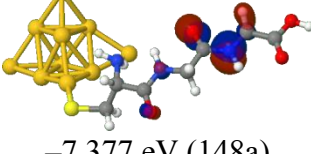
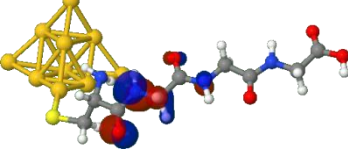
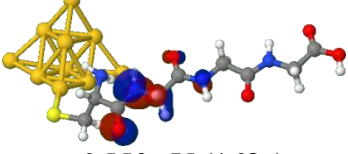
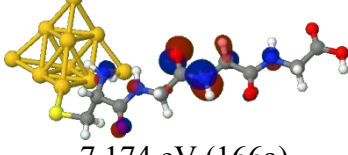
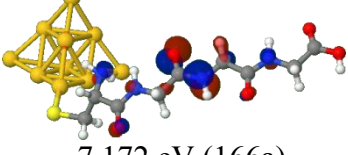
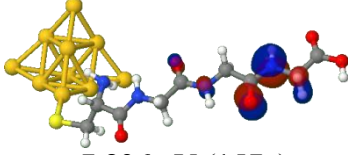
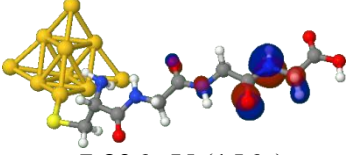
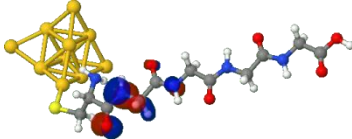
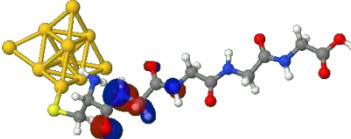
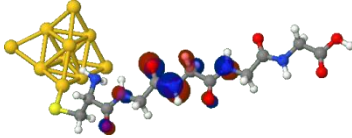
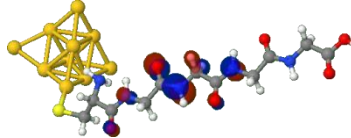
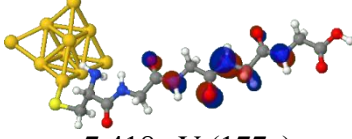
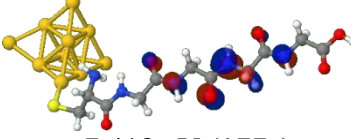
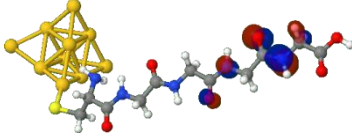
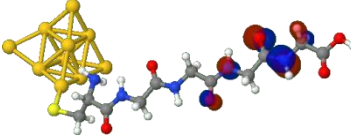
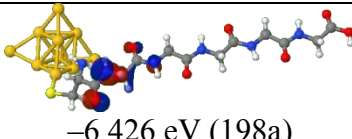
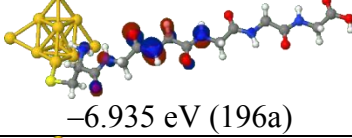
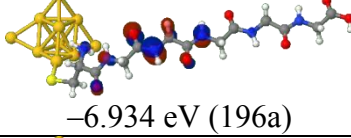
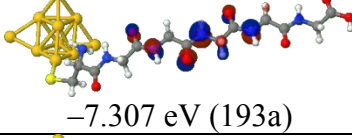
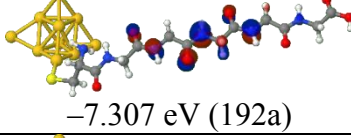
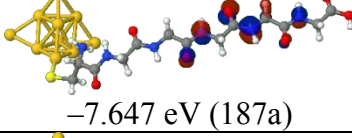
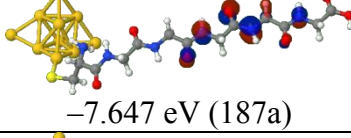
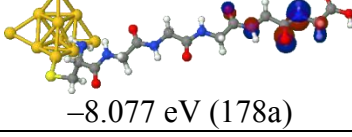
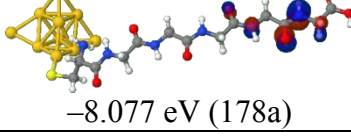
Compound	MO, N alpha	MO, N beta
Au ₁₀ CysGly	 -6.996 eV (138a)	 -6.996 eV (138a)
Au ₁₀ Cys(Gly) ₂	 -6.623 eV (153a)	 -6.623 eV (153a)
	 -7.378 eV (149a)	 -7.377 eV (148a)
Au ₁₀ Cys(Gly) ₃	 -6.551 eV (168a)	 -6.550 eV (168a)
	 -7.174 eV (166a)	 -7.172 eV (166a)
	 -7.836 eV (157a)	 -7.836 eV (156a)

Table S4 (continued).

Compound	MO, N alpha	MO, N beta
Au ₁₀ Cys(Gly) ₄	 -6.449 eV (183a)	 -6.449 eV (183a)
	 -6.998 eV (181a)	 -6.998 eV (181a)
	 -7.418 eV (177a)	 -7.418 eV (177a)
	 -7.857 eV (170a)	 -7.857 eV (167a)
	Au ₁₀ Cys(Gly) ₅	 -6.426 eV (198a)
 -6.935 eV (196a)		 -6.934 eV (196a)
 -7.307 eV (193a)		 -7.307 eV (192a)
 -7.647 eV (187a)		 -7.647 eV (187a)
 -8.077 eV (178a)		 -8.077 eV (178a)

DFT-Derived Parameters of Superexchange Tunneling Model. The superexchange tunneling model considers a linear arrangement of localized orbitals coupled through nearest-neighbor interactions. (28-30) Due to symmetry, the in-plane and the out-of-plane occupied orbitals of the amide groups can be considered independently in the extended configuration (See Fig. 4C of the manuscript). Additionally, the lone pair orbitals of the terminal NH₂ and COOH groups interact with the in-plane orbitals of the amide groups. Within each orbital manifold, a simple Hückel-type model including only nearest-neighbor couplings is applicable, so that the energy eigenvalues are determined by eq. S1.

$$e_j = e_0 + 2V \cos\left(\frac{j\rho}{n+1}\right) \quad \text{eq. S1}$$

In eq. S1, the index j denotes the orbital index within the manifold, n is the total number of interacting orbitals, and ε_0 and V give the energies of the localized orbitals and the strengths of nearest-neighbor interactions, respectively. (28, 31) We estimated the tunneling model parameters ε_0 and V by fitting the orbital energies obtained from DFT calculations to the above analytical expression. The fits for the in-plane and out-of-plane occupied orbitals of the Au₁₀Cys(Gly)_n (n = 1-5) series are given in Fig. S12 and S13.

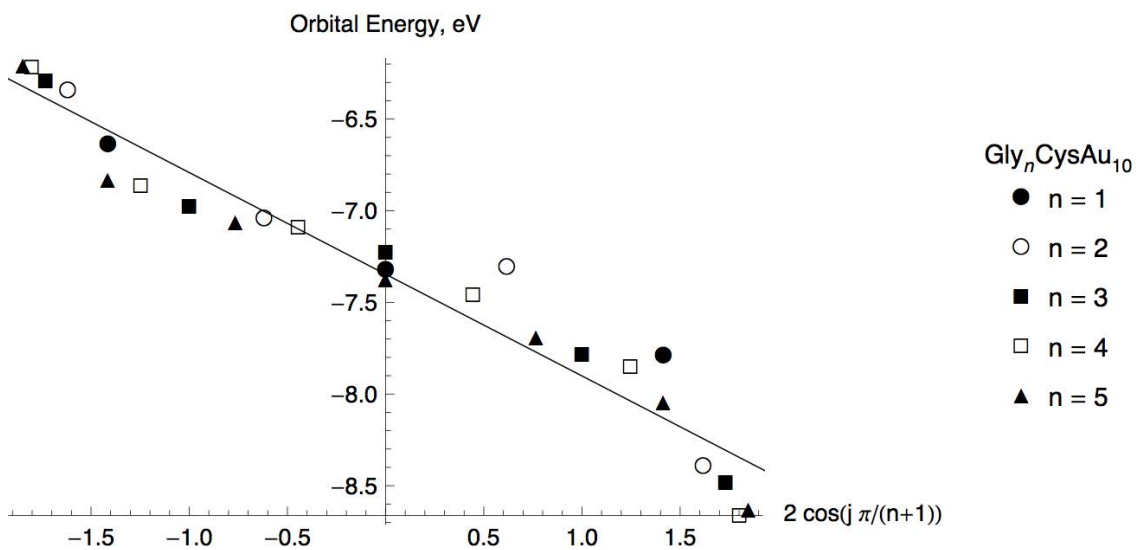


Fig. S12. Linear fit for the superexchange tunneling parameters and ϵ_0 and V of the in-plane occupied orbitals of the amide groups of the Au₁₀Cys(Gly)_n (n = 1-5) series. See text for further explanations.

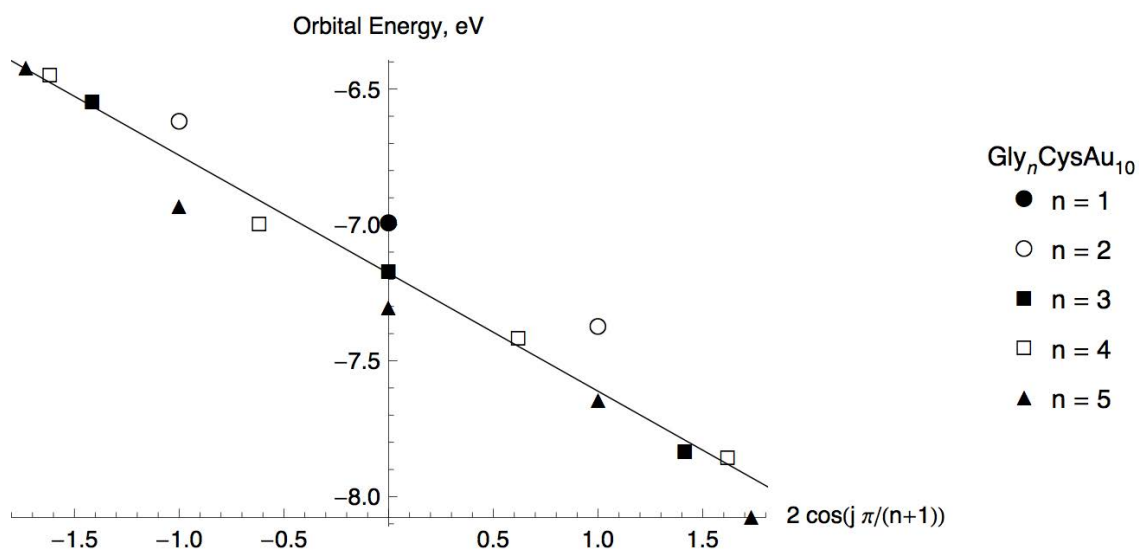


Fig. S13. Linear fit for the superexchange tunneling parameters and ε_0 and V of the out-of-plane occupied orbitals of the amide groups of the Au₁₀Cys(Gly)_n (n = 1-5) series. See text for further explanation.

The results of the linear fits are $\varepsilon_0 = (-7.35 \pm 0.04)$ eV and $V = (-0.55 \pm 0.03)$ eV for the in-plane occupied orbitals of the amide groups and $\varepsilon_0 = (-7.18 \pm 0.03)$ eV and $V = (-0.43 \pm 0.03)$ eV for the out-of-plane orbitals. The average orbital energy of the sulfur lone pair orbital in the oligoglycine series—which we consider a lower bound for the Fermi energy ε_F here—is -5.69 eV.

The linear fits for the orbital energies of the in-plane occupied orbitals in the $\text{Au}_{10}\text{Cys}(\beta\text{-Ala})_n$ ($n = 1-3$) series are shown in Fig. S14. The result of the linear fit is $\varepsilon_0 = (-6.95 \pm 0.05)$ eV and $V = (-0.34 \pm 0.04)$ eV for the in-plane occupied orbitals of the amide groups. The out-of-plane occupied orbitals in the $\text{Au}_{10}\text{Cys}(\beta\text{-Ala})_n$ ($n = 1-3$) series show very small energy splittings and do not fit a simple superexchange model. For compound **25**, the linear fit for in-plane occupied orbitals of the amide groups yields $\varepsilon_0 = (-6.96 \pm 0.05)$ eV and $V = (-0.38 \pm 0.04)$ eV. For in-plane occupied amide orbitals in compound **26**, we obtained $\varepsilon_0 = (-6.92 \pm 0.02)$ eV and $V = (-0.35 \pm 0.02)$ eV.

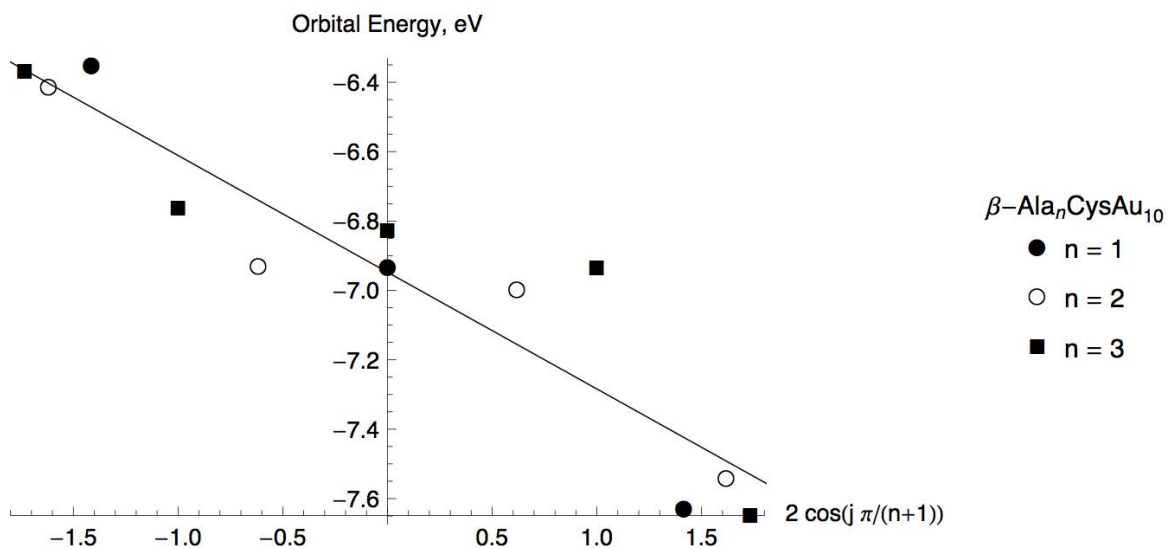


Fig. S14. Linear fit for the superexchange tunneling parameters and ε_0 and V of the in-plane occupied orbitals of the amide groups of the $\text{Au}_{10}\text{Cys}(\beta\text{-Ala})_n$ ($n = 1\text{-}3$) series. See text for further explanation.

Model for Tunneling Rates. The superexchange tunneling model gives an analytical expression for the tunneling decay coefficient β (eq. S2) (28)

$$b = \frac{2}{n_{\text{at}}} \ln \left(\frac{e_{\text{F}} - e_0}{|V|} \right) \quad \text{eq. S2}$$

which we can estimate using the DFT-derived parameters ε_0 and V . Using the parameters from the in-plane (ip) occupied orbitals of the $\text{Au}_{10}\text{Cys}(\text{Gly})_n$ ($n = 1-5$) series, we obtain $\beta_{\text{ip}} = (0.73 \pm 0.08) n_{\text{atom}}^{-1} ((0.62 \pm 0.09) \text{ \AA}^{-1})$, while the parameters for the out-of-plane (oop) orbitals are $\beta_{\text{oop}} = (0.82 \pm 0.09) n_{\text{atom}}^{-1} ((0.70 \pm 0.10) \text{ \AA}^{-1})$. The standard deviations were obtained from the uncertainties in the parameters ε_0 and V of the linear regressions in Figs. S12 and S13. The unit length of oligoglycines was determined from optimized molecular structures (see Table S5). These attenuation factors β , obtained from the superexchange model, are rough estimates as they do not take into account possible intermolecular and finite bias effects, and dynamic disorder. The relative contributions of these ip and oop orbital manifolds to tunneling depend on their overlaps with the orbitals of the metal electrodes and on the chain dynamics. The overall tunneling decay parameter β is a weighted sum of the contributions of the individual tunneling channels.

The values of $\beta = 0.6-0.7 n_{\text{atom}}^{-1}$ derived here, while lower than those for n -alkanethiols, are too high compared to the experimental values. The estimated tunneling decay coefficient β for the in-plane occupied orbitals in the $(\beta\text{-Ala})_n\text{CysAu}_{10}$ ($n = 1-3$) series is $\beta_{\text{ip}} = (0.64 \pm 0.09) n_{\text{atom}}^{-1} ((0.60 \pm 0.13) \text{ \AA}^{-1})$, which is close to the corresponding value for the oligoglycines. The estimated tunneling decay coefficients β decrease considerably with larger distances between the amide groups. A linear fit of orbital energies yields indistinguishable values of $\beta_{\text{ip}} = (0.49 \pm 0.08) n_{\text{atom}}^{-1}$

$((0.41 \pm 0.10) \text{ \AA}^{-1})$ and $\beta_{ip} = (0.42 \pm 0.04) n_{\text{atom}}^{-1} ((0.38 \pm 0.06) \text{ \AA}^{-1})$ for the compounds **25** and **26**, which contain 3 and 4 intervening CH₂ groups, respectively.

Interpretation of Nearest-Neighbor Interactions between Occupied Orbitals. The interaction between high-lying occupied orbitals of peptide groups is crucial to the superexchange model of tunneling through oligoglycines. Here, we discuss the underlying quantum mechanical effects in a qualitative manner, following the interpretation of Ruedenberg and co-workers. (32, 33) Starting from a detailed analysis of the bond formation in the hydrogen molecule, Ruedenberg and co-workers provide a useful qualitative picture various energetic contribution to chemical bonding. Briefly, the overlap between the neighboring orbitals creates delocalization along the axis that connects their centers but leads to localization in the direction perpendicular to it. The first effect is destabilizing for a pair of occupied orbitals, but the orbital contraction yields a stabilization that is crucial to the energetics of chemical bond formation. (32, 33) This argument is not limited to interactions between partially filled shells, which results in covalent bonding, but can also be applied to occupied orbitals, as is the case of the lone-pair orbitals of the peptide groups. Conventional wisdom dismisses these interactions as generally unfavorable, based on the example on the non-existent He₂ molecule and a simplified computational description of the orbital interaction (linear combination of atomic orbitals, minimal basis). In contrast, secondary interactions between occupied orbitals can be both destabilizing (steric repulsion) and stabilizing, depending on the balance between orbital delocalization along the molecular chain and orbital contraction perpendicular to it. These effects are well captured by modern quantum chemical methods such as DFT using flexible basis sets. The degree of delocalization of lone-pair orbitals of the peptide bonds in oligoglycines is discernible in Tables S3 and S4.

Table S5. Molecule lengths of oligopeptides from optimized structures using DFT in Å from sulfur atom to farthest COOH hydrogen atom.

Molecule ^a	Length, Å
2	8.78
3	13.05
4	15.96
5	20.38
6	22.80
22	9.64
23	12.98
24	18.64

^aThe numbers correspond to compounds in Fig. 3A.

Supplementary Text

Mechanism of Charge Transport. The simplified Simmons equation (Eq. 1), (34-36) which approximates a SAM-based junction as a rectangular tunneling barrier between two electrodes, models the observed exponential decrease in tunneling current density with increasing distance. Varying the thickness of the molecular structure (d , Å) and plotting $\log|J|$ vs. d yields a y intercept ($\log|J_0|$: i.e., $\log|J|$ when $d = 0$) and slope ($-\beta/2.303$, Å⁻¹ or per methylene, CH₂⁻¹, in n -alkanethiolates). From Eq.1, the value of the parameter J_0 , is the current for a hypothetical junction with interfaces characteristic of the SAM but with a SAM of zero thickness ($d = 0$), and β is the tunneling decay coefficient.

Charge Transport across Proteins/Peptides. CT through peptides has been studied with a variety of techniques:(37-40) examples include electrochemistry on SAMs of ferrocenoyl oligopeptides on metal surfaces,(41, 42) and scanning probe microscopy on a single molecule,(43) or small number of peptide molecules on a metal surface.(38) CT in peptides has been studied in some detail, also, in the context of donor-bridge-acceptor molecules by spectroscopic techniques.(44) Most of these studies agree that the structure of the peptide may influence the properties of CT.(19, 40, 45) Different groups have concluded that when the CT distance exceeds a certain value (e.g., the length required for the amino acids to develop secondary structure(45, 46)), the mechanism of CT changes from tunneling to other mechanisms characterized by a weaker distance-dependence than that characteristic of tunneling.(19, 44-46) Even in measurements of the rate of CT through short sequences of peptides, however, the results, produced using different methods (e.g., electrochemistry(47) and single-molecule studies(48)) are inconsistent.

Charge Transport across Oligoglycines. Using a single-molecule STM probe, Tao and coworkers carried out a study of CT across short (1–3 amino acids) oligopeptides connected to two gold electrodes.⁽⁴³⁾ Their study—using HS-(CH₂)₂-NH-(Gly)_n-Cys (where n = 0, 1, 2) and measuring conductance (*G*) versus number of atoms—gave similar values of β for peptides ($\beta = 1.1$ per non-hydrogen atom) and alkanedithiols ($\beta = 1.1$ per non-hydrogen atom).⁽⁴³⁾ Analysis of current densities showed that SAMs of oligoglycines (presented in Fig. 1) are more conductive by tunneling than SAMs of alkanethiolates. These results across SAMs of oligoglycines may differ from those determined using single molecule measurements (using HS-(CH₂)₂-NH-(Gly)_n-Cys, where n = 0, 1, 2)⁽⁴³⁾; this study indicated that the values of β for oligoglycines and alkanethiols were similar. This observation appears to be in contrast to that reported here; we measure significantly different values of β for alkanethiols and oligopeptides. There are, however, several possible differences between these sets of experiment.

i) The single-molecule studies use a junction of the form AuS-(CH₂)_nR(Gly)_nCysAu. We have demonstrated that the AuSR can influence the form of the tunneling barrier, and in Tao's work these are two such interfaces.⁽⁴⁹⁾ *ii) Single-molecule vs. large-area measurements.* Tao and coworkers use a single-molecule approach, and we use an ostensibly "large-area" junction (although the actual area of electrical contact is much smaller than the footprint of the junction).^(3, 50) The relative precision of the two techniques is not clear. The difference in the junction could appear in other ways, especially in the conformations of the molecules. *iii) Tao examined chains extending only to n = 2.* His results and ours differ by <factor of 10 for this length of (Gly)_n and depending on his experimental uncertainties, these results may or may not be statistically significant. (We are only confident that β is significantly different between the (Gly)_n series and *n*-alkane derivatives in the longer (Gly)_n derivatives).

Charge Transport across Amide-Containing SAMs using Ga₂O₃/EGaIn Top Electrode. We observed previously that the replacement of a *single* –CH₂CH₂– group with an amide group, –CONH– or –NHCO–, anywhere in the structure of an alkanethiolate had no detectable influence on the rate of charge transfer at V = 0.5 V.(51-54)

The Difference in the Values of J₀ could be due to the Extrapolation of Data. Unlike the value of β , which is determined directly from the data using eq. 1, the value of J_0 is estimated by extrapolation of the data to zero length (eq. 1, $d = 0$). This extrapolation gives only an *estimation* of J_0 , since it is derived outside of the range of data defined by the (Gly)_n; the shortest peptide, in our series, is CysGly, which has seven non-hydrogen atoms. We measured the current density for a series of molecules that are shorter than Cys (**4**), but have structures similar to Cys (**4**) (Fig. 2). These molecules fit to the extrapolated line derived for *n*-alkanethiolates (Fig. 2 and S8) rather than that defined by the (Gly)_n series. Based on current information, we cannot clearly define the value of J_0 for the oligoglycines, because a simple extrapolation over the (Gly)_n series may be (and in fact probably is) inappropriate for SAMs not containing a Gly unit.

These results point to an ambiguity that makes it more difficult to estimate values of J_0 for many systems of SAMs in which an important element of the structure is a repeating unit containing several atoms (here (Gly)_n or –NHCH₂CO–, but equally –C₆H₄– or oligophenylene, and –OCH₂CH₂– for oligoethylene glycol). Uniquely, A(CH₂)_nH (where A = HS–, HC≡C–, HO₂C–) can be studied with small values of *n* (for alkanethiolates on Au, *n* = 1 or perhaps *n* = 0); for these molecules J_0 can be defined without extrapolation.(3, 49, 55) By contrast, in our studies, for Cys(Gly)_n, *n* = 0 still has a chain of four non-hydrogen atoms whose properties are not exactly those of the three atoms of a Gly unit, and which may also interact differently with the orbitals in the interfaces with the electrode composed of AuS–. (Other work has demonstrated

that delocalization of the HOMO from the thiol unit out into the molecule making up the SAM can have an important influence on the structure of the tunneling barrier.)(56)

Acknowledgements

Sample characterization was performed at the Center for Nanoscale Systems (CNS) at Harvard University, a member of the National Nanotechnology Infrastructure Network (NNIN), which is supported by the National Science Foundation (ECS-0335765). In particular, we appreciate the assistance of Dr. Hao-Yu Lin at CNS with XPS analysis.

References and Notes

1. A. Kikuzawa, T. Kida, M. Akashi, Synthesis of stimuli-responsive cyclodextrin derivatives and their inclusion ability control by ring opening and closing reactions. *Org. Lett.* **9**, 3909 (2007).
2. X. Lu *et al.*, Designed semisynthetic protein inhibitors of Ub/Ubl E1 activating enzymes. *J. Am. Chem. Soc.* **132**, 1748 (2010).
3. F. C. Simeone *et al.*, Defining the value of injection current and effective electrical contact area for EGaIn-based molecular tunneling junctions. *J. Am. Chem. Soc.* **135**, 18131 (2013).
4. K. P. Fears, T. D. Clark, D. Y. Petrovykh, Residue-dependent adsorption of model oligopeptides on gold. *J. Am. Chem. Soc.* **135**, 15040 (2013).
5. O. Cavalleri *et al.*, High resolution X-ray photoelectron spectroscopy of L-cysteine self-assembled films. *Phys. Chem. Chem. Phys.* **6**, 4042 (2004).

6. S. Fischer *et al.*, L-Cysteine on Ag(111): A combined STM and X-ray spectroscopy study of anchorage and deprotonation. *J. Phys. Chem. C* **116**, 20356 (2012).
7. A. Shaporenko, A. Terfort, M. Grunze, M. Zharnikov, A detailed analysis of the photoemission spectra of basic thioaromatic monolayers on noble metal substrates. *J. Electron. Spectrosc.* **151**, 45 (2006).
8. P. Cyganik *et al.*, Competition as a design concept: Polymorphism in self-assembled monolayers of biphenyl-based thiols. *J. Am. Chem. Soc.* **128**, 13868 (2006).
9. K. P. Fears, D. Y. Petrovykh, T. D. Clark, Evaluating protocols and analytical methods for peptide adsorption experiments. *Biointerphases* **8** (2013).
10. O. Dannenberger *et al.*, An orientation analysis of differently endgroup-functionalised alkanethiols adsorbed on Au substrates. *Thin Solid Films* **307**, 183 (1997).
11. J. C. Love *et al.*, Formation and structure of self-assembled monolayers of alkanethiolates on palladium. *J. Am. Chem. Soc.* **125**, 2597 (2003).
12. W. K. Surewicz, H. H. Mantsch, New insight into protein secondary structure from resolution-enhanced infrared-spectra. *Biochim. Biophys. Acta* **952**, 115 (1988).
13. C. H. Bamford *et al.*, Structure of polyglycine. *Nature* **176**, 396 (1955).
14. M. Smith, A. G. Walton, J. L. Koenig, Raman spectra of polyglycines. *Biopolymers* **8**, 29 (1969).
15. V. D. Gupta, M. K. Gupta, K. Nath, Vibrational-spectra of oligomers of glycine in relation to polyglycine. *Biopolymers* **14**, 1987 (1975).
16. S. Bykov, S. Asher, Raman studies of solution polyglycine conformations. *J. Phys. Chem. B* **114**, 6636 (2010).

17. S. Ohnishi, H. Kamikubo, M. Onitsuka, M. Kataoka, D. Shortle, Conformational preference of polyglycine in solution to elongated structure. *J. Am. Chem. Soc.* **128**, 16338 (2006).
18. S. V. Bykov, S. A. Asher, UV resonance raman elucidation of the terminal and internal peptide bond conformations of crystalline and solution oligoglycines. *J. Phys. Chem. Lett.* **1**, 269 (2010).
19. S. Sek, A. Sepiol, A. Tolak, A. Misicka, R. Bilewicz, Distance dependence of the electron transfer rate through oligoglycine spacers introduced into self-assembled monolayers. *J. Phys. Chem. B* **108**, 8102 (2004).
20. C. M. Bowers *et al.*, Introducing ionic and/or hydrogen bonds into the SAM//Ga₂O₃ top-interface of Ag^{TS}/S(CH₂)_nT//Ga₂O₃/EGaIn junctions. *Nano Lett* **14**, 3521 (2014).
21. R. L. McCreery, A. J. Bergren, Progress with molecular electronic junctions: meeting experimental challenges in design and fabrication. *Adv. Mater.* **21**, 4303 (2009).
22. A. D. Becke, Density-functional thermochemistry .3. The role of exact exchange. *J. Chem. Phys.* **98**, 5648 (1993).
23. K. Eichkorn, O. Treutler, H. Ohm, M. Haser, R. Ahlrichs, Auxiliary basis-sets to approximate coulomb potentials. *Chem. Phys. Lett.* **240**, 283 (1995).
24. F. Weigend, R. Ahlrichs, Balanced basis sets of split valence, triple zeta valence and quadruple zeta valence quality for H to Rn: Design and assessment of accuracy. *Phys. Chem. Chem. Phys.* **7**, 3297 (2005).
25. F. Weigend, Accurate coulomb-fitting basis sets for H to Rn. *Phys. Chem. Chem. Phys.* **8**, 1057 (2006).

26. D. Andrae, U. Haussermann, M. Dolg, H. Stoll, H. Preuss, Energy-adjusted abinitio pseudopotentials for the 2nd and 3rd row transition-elements. *Theor. Chim. Acta* **77**, 123 (1990).
27. F. Furche *et al.*, Turbomole. *Wires Comput. Mol. Sci.* **4**, 91 (2014).
28. A. Nitzan, Electron transmission through molecules and molecular interfaces. *Annu. Rev. Phys. Chem.* **52**, 681 (2001).
29. R. Kosloff, M. A. Ratner, Superexchange-assisted through-bridge electron-transfer-electronic and dynamic aspects. *Israel J. Chem.* **30**, 45 (1990).
30. J. A. Hoerni, Application of free-electron theory to three-dimensional networks. *J. Chem. Phys.* **34**, 508 (1961).
31. L. Salem, *The molecular orbital theory of conjugated systems*. (W.A. Benjamin, New York,, 1966), pp. xvi, 576 p52.
32. K. Ruedenberg, Physical nature of chemical bond. *Rev Mod Phys* **34**, 326 (1962).
33. N. C. Baird, The chemical bond revisited. *J. Chem. Educ.* **63**, 660 (1986)34.
34. J. G. Simmons, Electric tunnel effect between dissimilar electrodes separated by a thin insulating film. *J. Appl. Phys.* **34**, 2581 (1963).
35. J. G. Simmons, Generalized formula for electric tunnel effect between similar electrodes separated by a thin insulator film. *J. Appl. Phys.* **34**, 1793 (1963).
36. J. G. Simmons, G. J. Unterkofer, Potential barrier shape determination in tunnel junctions. *J. Appl. Phys.* **34**, 1828 (1963).
37. S. S. Isied, M. Y. Ogawa, J. F. Wishart, Peptide-mediated intramolecular electron-transfer-long-range distance dependence. *Chem. Rev.* **92**, 381 (1992).

38. S. Sek, Peptides and proteins wired into the electrical circuits: An SPM-based approach. *Biopolymers* **100**, 71 (2013).
39. M. Cordes, B. Giese, Electron transfer in peptides and proteins. *Chem. Soc. Rev.* **38**, 892 (2009).
40. A. Shah *et al.*, Electron transfer in peptides. *Chem. Soc. Rev.* **44**, 1015 (2015).
41. Y. Arikuma, K. Takeda, T. Morita, M. Ohmae, S. Kimura, Linker effects on monolayer formation and long-range electron transfer in helical peptide monolayers. *J. Phys. Chem. B* **113**, 15900 (2009).
42. M. M. Galka, H. B. Kraatz, Electron transfer studies on self-assembled monolayers of helical ferrocenoyl-oligoproline-cystamine bound to gold. *ChemPhysChem* **3**, 356 (2002).
43. X. Y. Xiao, B. Q. Xu, N. J. Tao, Conductance titration of single-peptide molecules. *J. Am. Chem. Soc.* **126**, 5370 (2004).
44. R. A. Malak, Z. N. Gao, J. F. Wishart, S. S. Isied, Long-range electron transfer across peptide bridges: The transition from electron superexchange to hopping. *J. Am. Chem. Soc.* **126**, 13888 (2004).
45. S. Sek, A. Sepiol, A. Tolak, A. Misicka, R. Bilewicz, Distance dependence of the electron transfer rate through oligoglycine spacers introduced into self-assembled monolayers. *J. Phys. Chem. B* **108**, 8102 (2004).
46. J. X. Yu *et al.*, Electron transfer through alpha-peptides attached to vertically aligned carbon nanotube arrays: a mechanistic transition. *Chem. Commun.* **48**, 1132 (2012).
47. J. X. Yu, J. R. Horsley, A. D. Abell, The influence of secondary structure on electron transfer in peptides. *Aust. J. Chem.* **66**, 848 (2013).

48. J. Juhaniewicz, S. Sek, Peptide molecular junctions: Distance dependent electron transmission through oligoprolines. *Bioelectrochem.* **87**, 21 (2012).
49. D. N. Beratan, J. N. Onuchic, J. R. Winkler, H. B. Gray, Electron-tunneling pathways in proteins. *Science* **258**, 1740 (1992).
50. C. M. Bowers *et al.*, Characterizing the metal–SAM interface in tunneling junctions. *Acs Nano* **9**, 1471 (2015).
51. M. M. Thuo *et al.*, Replacing -CH₂CH₂- with -CONH- does not significantly change rates of charge transport through Ag^{TS}-SAM//Ga₂O₃/EGaIn junctions. *J. Am. Chem. Soc.* **134**, 10876 (2012).
52. H. J. Yoon *et al.*, The rate of charge tunneling through self-assembled monolayers is insensitive to many functional group substitutions. *Angew. Chem. Int. Ed.* **51**, 4658 (2012).
53. H. J. Yoon, C. M. Bowers, M. Baghbanzadeh, G. M. Whitesides, The rate of charge tunneling is insensitive to polar terminal groups in self-assembled monolayers in Ag^{TS}(CH₂)_nM(CH₂)_mT//Ga₂O₃/EGaIn junctions. *J. Am. Chem. Soc.* **136**, 16 (2014).
54. F. Mirjani, J. M. Thijssen, G. M. Whitesides, M. A. Ratner, Charge transport across insulating self-assembled monolayers: non-equilibrium approaches and modeling to relate current and molecular structure. *ACS Nano* **8**, 12428 (2014).
55. K. C. Liao, H. J. Yoon, C. M. Bowers, F. C. Simeone, G. M. Whitesides, Replacing (AgSCH₂)^{TS}-R with (AgO₂C)^{TS}-R in EGaIn-based tunneling junctions does not significantly change rates of charge transport. *Angew. Chem. Int. Ed.* **53**, 3889 (2014).

56. R. Cohen, K. Stokbro, J. M. L. Martin, M. A. Ratner, Charge transport in conjugated aromatic molecular junctions: Molecular conjugation and molecule–electrode coupling. *J. Phys. Chem. C* **111**, 14893 (2007).